Electronic structure of UN based on specific heat and field-induced transitions up to 65 T

R. Troć,[1] M. Samsel-Czekała,[1] A. Pikul,[1] A. V. Andreev,[2] D. I. Gorbunov,[2,3] Y. Skourski,[3] and J. Sznajd[1]

[1]*W. Trzebiatowski Institute of Low Temperature and Structure Research, Polish Academy of Sciences, Okólna 2, 50-422 Wrocław, Poland*

[2]*Institute of Physics, Academy of Sciences, Na Slovance 2, 182 21 Prague, Czech Republic*

[3]*Dresden High Magnetic Field Laboratory (HLD-EMFL), Helmholtz-Zentrum Dresden-Rossendorf, D-01314 Dresden, Germany*

(Received 18 July 2016; published 16 December 2016)

The $5f$ electrons of uranium in the uranium mononitride (UN) compound are described in the literature as either localized or fully itinerant. Motivated by these contradictory statements, we studied low-temperature specific heat and high-field magnetization of single-crystalline UN in magnetic fields up to 9 and 65 T, respectively. Our detailed analysis of the magnetic contribution to the specific heat of UN revealed that its real ground state is complex and the $5f$ electrons seem to have a dual nature; i.e., they possess simultaneously local and itinerant characters in two substates. High-field experiments allowed us to construct a tentative magnetic phase diagram of UN with a metamagnetic transition from antiferromagnetism to ferrimagnetism at a magnetic field as high as 58 T at 2 K. Such a field only enables a reversal of 1 of the 12 antiferromagnetically coupled ferromagnetic layers in the direction of the magnetic field. Any further steplike transitions require application of ever higher magnetic fields, which is beyond the experimental possibilities. We show that the magnetic phase diagram can be successfully reproduced considering a layer model of the Ising spins. That model allows rough estimation of a phase transition into fully induced ferromagnetism at a field as high as about 258 T. It gives rise to a giant coupling between ferromagnetically ordered layers in UN. The obtained characteristics are presented, together with the results of recent x-ray photoemission spectroscopy and transport property measurements. They are analyzed and compared with a number of earlier experiments and band structure calculations that were performed for this compound and are widely described in the literature. We show that different experiments probe different substates of the uranium $5f$ electrons in UN (itinerant or localized), which supports our hypothesis on their dual nature.

DOI: 10.1103/PhysRevB.94.224415

I. INTRODUCTION

Uranium mononitride (UN) has been intensively studied by numerous researchers worldwide because of its interesting physical, thermodynamic, and technological properties. A wealth of theoretical and experimental data is available. Most data were reviewed in *Landolt-Börnstein Numerical Data* in 2006 [1] (see references therein).

From the technological point of view, UN attracts much interest. Its high values of thermal conductivity (ThC) ($23\,\mathrm{W\,mK^{-1}}$), melting point (2850 °C), fuel density ($14.32\,\mathrm{g\,cm^{-3}}$), and temperature for crystal structure stability have made this nitride a promising advanced fuel material for future fourth-generation fast breeder reactors. However, in spite of a large number of existing experimental data obtained for UN using a variety of theoretical and experimental methods, there are still questions regarding the character of the $5f$ electrons in this simple nitride.

Uranium mononitride, crystallizing in the NaCl-type crystal structure, exhibits antiferromagnetic (AFM) ordering below $T_N = 51$–53 K, classified as AFM type I-1**k**. The expected tetragonal distortion associated with an AFM order of this type turned out to be very small ($|c/a - 1| = 6.5 \times 10^{-4}$ at 4.2 K). The ordered and effective moments were found to be $0.75\mu_B$ and 2.65–$3.10\mu_B$, respectively. In addition, it was observed that the distribution of the three possible domains with their ordered moments along the [100] and equivalent [010] and [001] crystal axes are almost equal to one another [2]. Hence, the directional anisotropy of the susceptibility or thermal strain measured along the three equivalent axes is very small. Therefore, the strain scales accurately with a square of the sublattice magnetization m_U. The various values of the reported effective moment, μ_{eff}, are primarily dependent on the value of the paramagnetic Curie point, θ_p, which has been estimated in the literature from the Curie-Weiss law, which is approximately followed only to room temperature (RT). Surprisingly, θ_p reaches highly negative values, varying between -250 and -310 K depending on the particular measurement and the corresponding extrapolation (see Table II A in Ref. [2]). Taking into account the modified Curie-Weiss law applied to the susceptibility data measured up to 1000 K, these parameters are slightly changed. Moreover, the above-mentioned parameters in the paramagnetic region are comparable to those found for ionic UO_2 [3]. So far, none of the numerous authors engaged in the study of UN have tried to explain that convergence. In addition, the neutron diffraction study of the $UN_{1-x}C_x$ solid solutions indicated a rapid decrease of T_N to 0 K with an increase of the carbon content only up to $x = 0.14$ [4]. This demonstrates how UN antiferromagnetism depends strongly on the nearest-neighbor environment around the uranium atom.

In the past, the U $5f$ electrons in UN were considered to be of either a localized (U^{3+}/U^{4+}) or a fully itinerant (U^{6+}) type. The first theoretical model explaining UN behavior and the other monopnictides or monochalcogenides was presented by Grunzweig-Genossar *et al.* [5]. This model, based on the localized U *5f* electrons, enabled the authors to calculate the magnetic moments in the ordered state and the susceptibilities in the paramagnetic state. The computed total splitting of the crystal field (CF) levels of the ground multiplet $^3H_4$ ($5f^2$ configuration) in UN was found to be about $\Delta_{CF} = 720$ K. The localized type was also deduced from the neutron form factor [6], CF characterization [7], and electrical and thermal transport properties [8]. In contrast, the

itinerancy of all $5f^3$ electrons was inferred from numerous band structure calculations (see references below) or from such experiments as inelastic neutron scattering [9] and photoemission [10] or magnetic study under pressure [11]. Still following the Grunzweig-Genossar *et al.* model [5], Lemmer and Lowther [7] analyzed the ordered and paramagnetic states in UN, assuming that the uranium ion is in the $U^{4+}(5f^2)$ tetravalent state. According to these authors, such a configuration satisfactorily accounts for the temperature dependence of the sublattice magnetization $m_U(T)$ of UN in the ordered region (experimental $m_U(T)$ dependence was taken from Ref. [6]) as well as the paramagnetic susceptibility between T_N and 1000 K (given in Ref. [12]). Unfortunately, the inelastic neutron scattering results [9] only indicate that the magnetic response at low temperatures is spread over a considerable frequency range centered on (110), with an anisotropy gap of 3.5 THz (170 K). Although UN is cubic, large anisotropy was also manifested in its critical neutron scattering [13].

It seems that the predominantly itinerant viewpoint on UN antiferromagnetism has been assumed by many authors (see below) because of the uranium interatomic distance ($d_{U\text{-}U}$, $= 0.34$ nm) in the NaCl-type crystal structure that is situated almost exactly on the Hill limit (∼0.34 nm) [14], which usually signals a crossover to full itinerancy of the $5f$ electrons and a possible occurrence of superconductivity. However, in the interplay between the hybridization of the $5f$ states with other states and their tendency to full itinerancy, the on-site coulomb correlation in uranium compounds even for such a short U-U distance is always predominant, leading at least to localization of two $5f$ electrons (instead of three), except for in a few examples, such as the case of uranium metal [15] or UB_2 and UB_{12} [16], all of which have typical metallic properties. The best example of the localization of $5f$ electrons even when the U-U distances are 0.33 nm is β-UH_3 (see Figs. 5 and 8 in Ref. [17]). The observed strong broadening of the photoemission spectrum of this trihydride is caused primarily by the correlation effect preferring to stabilize the final multiplets. Therefore, many outstanding aspects of UN behavior are still to be explained. In addition, we are dealing with a complex case that cannot be presented in a simple way, if one bears in mind all existing data up to now on the physical properties of UN (see, e.g., Refs. [1] and [8]).

To enhance our knowledge about this nitride, we present here experimental data obtained on a single-crystalline sample in detailed measurements of the specific heat and magnetization under magnetic fields up to 9 and 65 T, respectively. These data give support to considering UN as a dual $5f$ electron system (and/or intermediate valence system). In addition, we have used a molecular field approximation to predict roughly a magnetic phase diagram of UN.

II. EXPERIMENT

Measurements were performed on single crystals, selected from a batch of material obtained from the Battelle Memorial Institute, Columbus, Ohio. Ingots were prepared by nitriding a consumable electrode of depleted uranium under high pressure, and these had a resultant structure of UN with a slight quantity of U_2N_3. Therefore, the ingot was subsequently annealed for 8 h at 1500 °C in a 10^{-5} Torr vacuum to decompose the U_2N_3.

The x-ray photoelectron spectroscopy (XPS) study of obtained single crystals of UN was performed earlier, and the results are given in Ref. [8]. Here, it was important to determine the relative concentrations of the constituents in the studied single crystal. Thus, the Multipak Physical Electronics program [18] was used, enabling quantification of the XPS spectra utilizing the peak area and sensitivity factor. The Gaussian-Lorentzian functions were used to fit the XPS core-level spectra. The standard atomic concentration calculation provides a ratio of each component to the sum of all elements taken into account in the data. The elements are detectable, with a detection limit of 0.1 at.%. For good quality of the spectra, only those elements for which the specific line was clearly visible in the spectrum were considered. For these lines, the background individually selected in the region limited to the particular line was subtracted; after that, the integration of the peak area was performed. Analyzes of these crystals indicated near stoichiometry (a typical U/N atomic ratio of 1.01), an oxygen content of 290 ppm wt, and a carbon content of 30 ppm wt. The lattice parameter $a = 0.4890(1)$ nm. The crystals were oriented by x-rays using the backreflection Laue technique, and samples for the various measurements were cut using a saw made up of a thin tungsten wire.

Specific heat of the single-crystalline sample of UN in the form of a cube with a mass of 30.6 mg was measured by the thermal relaxation method in a commercial Quantum Design Physical Property Measurement System (PPMS) platform in the temperature range 2–300 K. The samples were glued to the holder using Apiezon N vacuum grease, the specific heat of which was measured earlier and carefully subtracted. The specific heat of the single crystal was also measured under magnetic fields that were varied from 0.5 to 9 T and applied parallel to the [100] axis.

High-field experiments were performed at the Dresden High Field Laboratory. The magnetization was measured in a pulsed magnetic field up to 65 T applied along the three main crystallographic directions of the cubic crystal, with a side length of 2 mm. The samples were cut into parallelepipeds and oriented with the longest edges parallel to the principal axes. The magnetization signal was obtained by integrating the voltage induced in a pickup coil system surrounding the sample. A detailed description of the measurement system is presented in [19]. The rise time of the magnet pulse was 40 ms, and the total pulse duration was 150 ms. The measurements were carried out at 2, 20, 40, and 60 K.

III. ELECTRONIC STRUCTURE

A. Band structure calculations and photoemission

In general, it is crucial in the prediction of electronic properties of any actinide compound to recognize the nature and role of the U $5f$ electrons. As we will point out below, because of their complex behavior in UN, this problem remains a challenge. A number of papers have presented the results of band structure calculations of UN within the density functional theory (DFT) in the local density approximation (LDA) or local spin density approximation (LSDA) (see, e.g., Refs. [1]

and [8]). Then, to treat electron-electron correlations existing in UN, a generalized gradient approximation (GGA) was applied (see, e.g., Refs. [20] and [21]). For more adequate treatment of the previously mentioned electron-electron correlations, the GGA + U functional has been employed by Gryaznov *et al.* [22], who take an optimal effective Hubbard parameter $U_{\text{eff}} = 1.85$ eV. They obtained fully relativistic results, which were in agreement with experimental data as to the magnetic moment and the ground state of the AFM order. However, it turned out that much lower values of U_{eff} stabilize the ferromagnetic (FM) order. These calculations also revealed an instability of a UN cubic unit cell with respect to a tetragonal distortion, where $c/a < 1$ for the AFM state and $c/a > 1$ for the FM one. The former case was confirmed by the experiment [1].

Both the older and the more recent calculations are based on treating all three U $5f$ electrons as mainly itinerant. However, it was shown in 2002 that so-called dual model [23] considers a more complex manifold of competing localized and delocalized $5f$-electron configurations on equal footing, which allows for a quantitative description of the low-energy part of the spectra. In general, they exhibit both dispersive quasiparticle peaks and incoherent local excitations. The latter, as shown in angle-resolved photoemission spectroscopy (ARPES) studies of some number of uranium compounds, usually appear as a spectral weight in the range of 0.1–0.5 eV binding energy (BE), which in turn reflects the existence of $5f$ final multiplets. Nevertheless, due to hybridization with broad conduction bands, these local states lying near Fermi level (E_{F}) experience slight energy dispersion, which distinctly enhances the density of states (DOS) at E_{F}. This is observed in the electron specific heat coefficient $\gamma(0)$, which was found for UN to be 49.6 mJ mol^{-1} K^{-2} [24]. Usually, the magnitude of that dispersion is beyond the available energy resolution of the spectra, i.e., below about 10–15 meV. In turn, a strongly dispersive band is found on the higher BE side, probably with some $5f$ character, as obtained in calculations [8]. Only now it becomes clear that the relatively narrow spectral peak situated close to E_{F} in numerous XPS data of uranium compounds, like that in our paper on UN (see Fig. 3 in Ref. [8]), though in good agreement with LDA calculations, in reality reflects a local multiplet structure in accordance with the ARPES experiment; see, e.g., Ito *et al.* [25] or Durakiewicz [26], as discussed below. Some evidence of the complex character of the $5f$ electrons in UN is reflected particularly in the corresponding $4f$-core-level spectrum, which is presented in Refs. [8] and [27]. It happens that our results [8] became more structural due to probing of a pure single crystal with a large residual resistivity ratio (RRR = 850) and considerably better resolution.

Such a dual nature of the U $5f$ electrons assumed in the theoretical model calculations for UN has been considered in only a few papers. Some examples dealing with this model are presented below. As concerns modern full-potential and full-relativistic calculations carried out beyond DFT for UN, only Petit *et al.* [28], Yin *et al.* [29], and Sun *et al.* [30] applied in some manner such an approach to the $5f$ electrons in UN. The results of Petit *et al.* [28] obtained by the self-interaction corrected, local spin density (SIC-LSD) method revealed some difficulty in distinguishing between fully itinerant (f^0) and partly localized (f^1or f^2) characters of the $5f$ electrons. Namely, the above f^n (where $n = 0,1$, and 2 and denotes the number of the localized electrons taken into account) configurations yielded similar ground state energies. Nevertheless, the global minimum was achieved for the f^1 configuration, as in the case of UPt_3 [31]. Therefore, the authors concluded that the valence state is a mixed configuration of f^0 and f^1. In addition, Yin *et al.* [29], based on a combination of DFT within local density approximation and dynamical mean-field theory (LDA + DMFT), obtained for nonmagnetic UN a predominant delocalization of the $5f$ electrons but also evidence of their partial localization. The above authors compared their results to our previous XPS results [8] and found good agreement with our experiment. Also, Sun *et al.* [30] performed LDA + DMFT calculations considering both nonmagnetic and hypothetical FM UN and obtained for these two phases typical Fermi liquid behavior; in addition, the narrow $5f$ peak was found to be slightly farther from E_{F} in comparison with the results of pure LDA.

Former ARPES experiments for UN (and for USb) made by Reihl *et al.* [32] and later by Ito *et al.* [25] have revealed a dual character of the $5f$ electrons. In particular, the latter authors exhibited the presence of two nondispersive U $5f$ bands near the Fermi level, instead of highly dispersive U $5f$-$6d$ hybridized bands predicted by their LDA calculations. These two narrow $5f$ bands, found distinctly for USb as well (see also Ref. [33]), may originate, e.g., from the U $5f^1$ final-state multiplets $^2F_{5/2,7/2}$ of tetravalent U^{4+} states, showing some localized nature of the $5f$ electrons, like those in UO_2 [34]. The latter are situated farther from the Fermi level than those in UN. Nonetheless, a marked contribution of these narrow $5f$ bands to the DOSs at E_E is responsible for metallic behavior, by forming with other electrons the conduction bands and hence the Fermi surface (FS) of UN in accordance with experiments, as described below. Similarly, recent ARPES measurements for UN by Durakiewicz [26] have revealed two narrow $5f$ bands near E_{F}, with a possible slight dispersion but one that is hardly discernible even in the available experiment with a high-energy resolution of 10–15 meV. The presence of the peak close to E_{F} has also been inferred from ultraviolet photoelectron spectroscopy (UPS) measurements performed on thin films of UN under ultra-high vacuum by Black *et al.* [35]. Our newly interpreted single-crystalline XPS data for UN [8] indicate only a partial broad contribution of itinerant $5f$ electrons to both the N $2p$ valence band (*f-p* hybridization) and the conduction one (*f-d* hybridization), presented in Fig. 3 of Ref. [8], while the remaining $5f$ electrons become localized in the vicinity of E_{F}, though only one fairly broad peak of high intensity was observed, which is probably an effect of smearing by the energy resolution of two narrow peaks observed in the ARPES measurements [25,26]. The hybridization of the f states with the p and d states contributes to the increase of the intersite exchange interaction, which in consequence promotes the AFM local state with giant anisotropy, as we will point out later using high-field magnetization measurements of a single-crystalline sample of UN.

B. Fermi surface

The nonmagnetic FS of UN has been calculated based on our previous band structure results [8], obtained by the fully

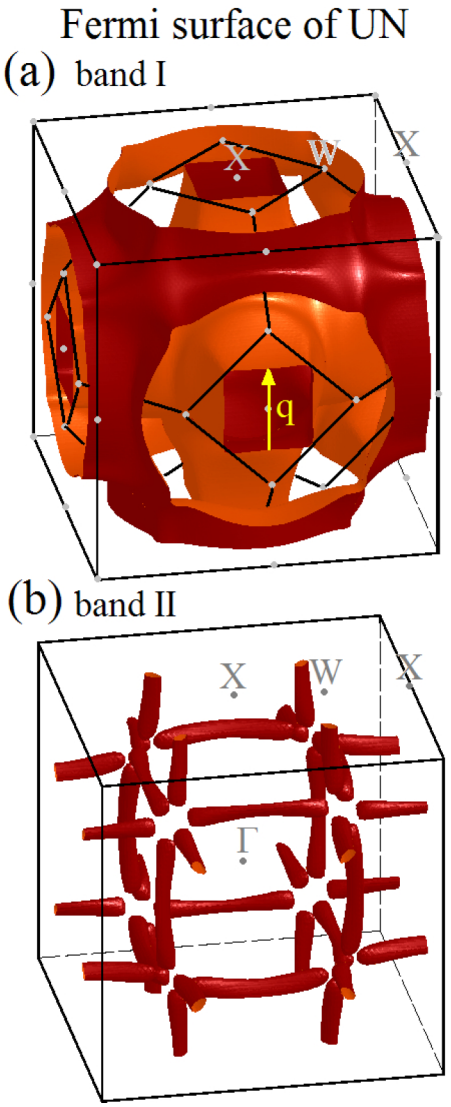

FIG. 1. Calculated FS sheets of UN, originating from Kramers double degenerate conduction bands I and II, displayed in (a) and (b), respectively. The nesting vector **q**, marked by the arrow on the holelike sheet in (a), is described in the main text.

relativistic FPLO code [36] within LDA (PW92) [37]. The obtained FS, visualized in Fig. 1, contains two (large and small) sheets originating from two conduction bands. The small one, coming from the upper band, consists of only electron cigars. The other one, derived from the lower band, contains a holelike structure that is open along the ΓX line (i.e., along the three equivalent crystal axes [100] = [010] = [001] in the face-centered-cubic [fcc] unit cell). This FS sheet along the ΓX direction and parallel ones exhibit nesting properties, with vectors (marked in Fig. 1) that have a length equal to $0.5|\Gamma X|$. Thus, the nesting vector may be responsible for arising spin density wave (SDW) fluctuations along the main crystallographic axes, possibly coexisting with the local AFM order. This question has yet to be clarified. Nevertheless, based on inelastic neutron scattering, the three-dimensional magnetic fluctuations below T_N in UN have already been reported [9]. Their presence was also revealed in electrical resistivity as

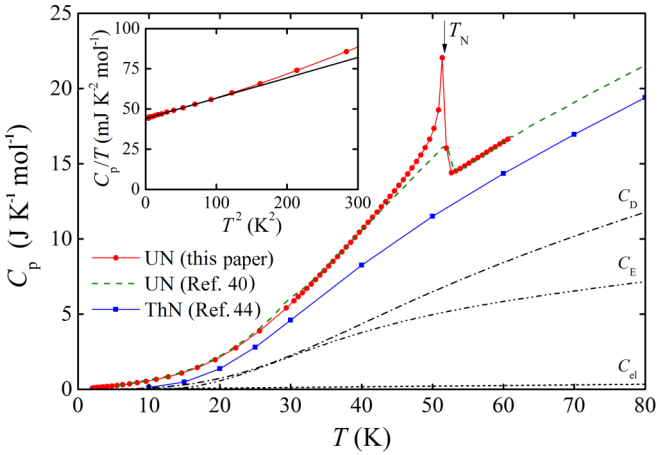

FIG. 2. Specific heat C_p of UN (solid circles), compared to that of Ref. [40], and ThN (solid squares). The latter (taken from Ref. [44]) is decomposed into the phonon (C_D and C_E) and electronic (C_{el}) parts. The inset shows the C_p/T vs T^2 function for UN.

a bump observed just below T_N (see Refs. [38] and [39] but especially Fig. 7 of Ref. [8], where such features were found along three main crystallographic directions). However, the origin of this type of fluctuation has not yet been explained. Our FS nesting seems to be robust and spans larger surface areas than the corresponding one considered for the same FS sheet and presented in Fig. 2(d) of Ref. [10]. The latter sheet was obtained by a different method employing an older LDA version (von Barth–Hedin) and was smeared by the energy resolution function and other simulated ARPES effects. Our results seem to describe better the FS cuts mapped by the ARPES measurements, displayed in Fig. 4(a), than their simulation, drawn in Fig. 4(b), of Ref. [10].

IV. EXPERIMENTAL RESULTS

A. Specific heat

In Fig. 2, we first show the temperature dependence of the specific heat, $C_p(T)$, of UN in a zero magnetic field compared to the results reported by Westrum and Barber [40]. The data were obtained on single-crystalline and polycrystalline samples, respectively. Good accordance between these two measurements is seen except for the temperature range of the occurrence of the AFM transition at the Néel point.

Contrary to Ref. [40], our results display a prominent sharp peak at $T_N = 51.2$ K. In addition, an anomaly observed at $T_N \approx 50$ K on an undefined UN sample by Yoshizawa and Suzuki [41] is considerably smaller than that seen in our measurements. This result shows that our sample of UN is of very good quality. From the low-temperature data (2–11 K) of C_p/T(UN) plotted against T^2 (see the inset of Fig. 2), we obtained the Sommerfeld coefficient $\gamma(0) = 45(1)$ mJ mol^{-1} K^{-2} and $\Theta_D{}^* = 313(5)$ K. These values are close to those reported in Ref. [24] [49.6 mJ mol^{-1} K^{-2} and 324(7) K, respectively], determined on the heat-treated polycrystalline sample in the temperature range 1.3–4.6 K. No nuclear specific heat at temperatures down to 1.3 K is expected for UN, because depleted uranium was used in the

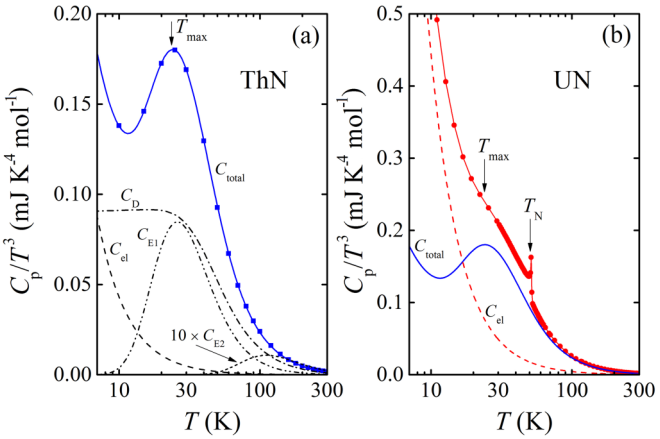

FIG. 3. Decompositions of the C_p/T^3 vs T functions of (a) ThN into C_D,C_{E1},C_{E2}, and C_{el}, while for (b) there is shown such a function for UN and a contribution of C_{el} (dashed line). Moreover, this subfigure shows a comparison with such a function of ThN (solid line).

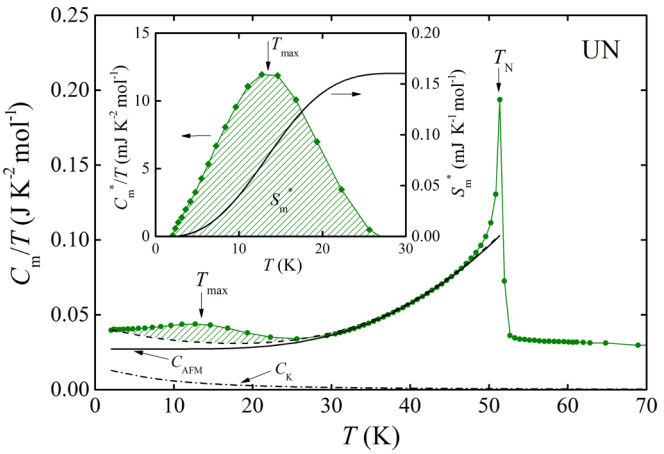

FIG. 4. Magnetic specific heat part of UN divided by temperature, C_m/T vs T. The solid line displays a spin wave fitting according to Eq. (2), while the dot-dashed line presents some Kondo-like contribution (see the text). The liner area indicates the presence of an additional contribution to the specific heat of UN, which probably has an SDW-like nature. The inset shows this SDW-like part, extracted from the total specific heat of UN, where the solid curve demonstrates the temperature change of entropy (right-hand scale).

preparation. However, we should treat $C_p(T)$ below 11 K as following the formula $C_p(T) = \gamma(0)T + (\beta_{ph} + \beta_m)T^3$, where the phonon part $\beta_{ph} = 12\pi/5r\Theta_D{}^{-3}$ (where $r = 2$ is a number of atoms per a formula unit), while β_m represents the magnetic part. Hence, the above value of $\Theta_D{}^*$ is calculated with the assumption that the contribution from the AFM ordering is negligible (i.e., $\beta_m \approx 0$) at such low temperatures. As we will show below, the specific heat attributed to excitations over a gap Δ_m in the AFM spin wave spectrum also has T^3 dependence. This likely causes its contribution to the C_p/T vs T^2 dependence at low temperatures. It seems that Θ_D inferred from the elastic behavior of UN, amounting to 282 K [42] or 291 K [43], is more appropriate and hence close to that value determined from specific heat measurements of ThN (284 K [44]).

In Fig. 2, we have also plotted the $C_p(T)$ function of the isomorphic nonmagnetic ThN given in Ref. [44]. As seen from this figure, that function can be expressed as a summation of three terms: the Debye $C_D(T)$, Einstein $C_E(T)$, and electronic $C_{el}(T)$ contributions (see below). To determine these contributions, the $C_p(\mathrm{ThN})/T^3$ vs T dependence was deconvoluted and delineated in Fig. 3(a).

As shown, this function goes through a maximum at T_{max}, indicating that except for the acoustic modes, this primarily contains contribution from the optical ones. The fitting has allowed attribution of $\Theta_D(\approx 242\,\mathrm{K})$ and two Einstein temperatures: $\Theta_{E1}(=128\,\mathrm{K})$ and $\Theta_{E2}(=548\,\mathrm{K})$. Only the latter one, of a small intensity, corresponds to that found in the neutron scattering experiment on the polycrystalline UN sample, namely, 494(7) K [45]. Both Danan *et al.* [44] and Yoshizawa and Suzuki [41] extracted similar Θ_E values from their specific heat measurements. In the literature [see, e.g., Refs. [46] and [47] and references therein], there are data of advanced neutron spectroscopy measurements of the vibrational excitations detected in a UN single crystal. As a result, the authors have found several sharp features corresponding to acoustic and optical one-phonon modes, in addition to the usual many-phonon excitations that have a weak and featureless response. The former modes characterize independent motions of light nitrogen atoms closed in an octahedral cage of heavy uranium atoms. By fitting the experimental data to the $C_p(\mathrm{ThN})/T^3$ vs T curve, we also estimated a value of the electronic coefficient of specific heat, $\gamma(0)$ ($\sim$4 mJ mol^{-1} K^{-2}), which is close to that of 3.12 mJ mol^{-1} K^{-2} given in Ref. [44] for ThN. Finally, these literature data have enabled estimation of the temperature dependence of the phonon contribution, $C_{ph}(\mathrm{UN})$, from the expression assuming three significant modes in the lattice, i.e.,

$$\begin{aligned} C_{ph}(\mathrm{UN}) &\approx C_p(\mathrm{ThN}) - C_{el}(\mathrm{ThN}) \\ &= (d_1/3)C_D(\Theta_D) + (d_2/3)C_{E1}(\Theta_{E1}) \\ &\quad + (d_3/3)C_{E2}(\Theta_{E2}) \end{aligned} \tag{1}$$

where $C_D(\Theta_D)$,$C_{E1}(\Theta_{E1})$, and $C_{E2}(\Theta_{E2})$ stand for conventional Debye and Einstein formulas for one atom, which is equivalent to three phonon branches (for details, see, e.g., Ref. [48]). However, there are only two atoms in the formula unit (which gives only six phonon branches available in total). Therefore, we had to introduce fractional values of degeneracy $d_1/3$, $d_2/3$, and $d_3/3$ as fitting parameters with a boundary condition: $d_1 + d_2 + d_3 = 6$. Satisfactory quality of the deconvolution of the phonon spectrum [presented in Fig. 3(a)] was obtained for $d_1 = 2$,$d_2 = 1$, and $d_3 = 3$. In Fig. 3(b), we display the $C_p(\mathrm{UN})/T^3$ vs T dependence, where for comparison we have also plotted a dependence of ThN such as that shown in Fig. 3(a). It is apparent from this figure that in spite of the AFM ordering and a high value of $\gamma(0)$, the presence of a shoulder at T_{max}, caused by the Einstein specific heat contribution, is seen in the case of UN.

The magnetic specific heat, treated here together with the electronic specific heat, divided by temperature, C_m/T, of UN, is plotted in Fig. 4. As usual, C_m was found by a subtraction of C_{ph} [established above by using the expression in Eq. (1)] from $C_p(T)$ of UN.

In the magnetically ordered region, one can see that except for a sharp peak at T_N, there is a small diffused peak at $T = 12$ K detected in the specific heat curve. Its presence in the case of UN will be discussed later in connection with the occurrence of similar anomalies in thermoelectric power (TEP) and thermal conduction. With the aim of extracting this anomaly from the C_m/T vs T curve, we have made fitting of its data taken between 28 and 46 K to the expression for AFM spin waves:

$$C_m/T = \gamma(0)^* + AT^2\exp(-\Delta_m/T) \tag{2}$$

with the following parameters: $\gamma(0)^* = 27(1)$ mJ mol^{-1} K^{-2}, $A = 1.24(3) \times 10^{-4}$ mJ mol^{-1} K^{-4}, and $\Delta_m = 75(2)$ K. The increase of C_m/T at $T = 0$ K by 18 mJ mol^{-1} K^{-2} [see $\gamma(0)$ above] has been assumed to originate from other contributions, such as a Kondo-like interaction with $T_K = 21$ K, as visible in Fig. 4. T_K has been found by using an expression given in the literature [49]. The problem of the presence of a Kondo-like interaction in UN is discussed below. Next, this procedure allowed us to extract a pure small peak starting at characteristic temperature $T^* \approx T_N/2$ (shown in the inset of Fig. 4) and determine its magnetic entropy $S_m{}^*$, which is equal to 0.16 J mol^{-1} K^{-1}. Furthermore, we have treated the C_m/T excess in the paramagnetic region T_N–300 K roughly estimated as being of the Schottky-type contribution described by the formula in Eq. (3) (see, e.g., Ref. [50]):

$$C_{\mathrm{Sch}}(T) = R\left[\frac{\sum_i g_i e^{-\frac{E_i}{T}} \sum_i g_i E_i^2 e^{-\frac{E_i}{T}} - \left(\sum_i g_i E_i e^{-\frac{E_i}{T}}\right)^2}{T^2\left(\sum_i g_i e^{-\frac{E_i}{T}}\right)^2}\right] \tag{3}$$

where R is a gas constant, E_i is the energy expressed in Kelvins, and g_i is the degeneracy of the energy level. The electronic contribution was neglected in this approach. This procedure yields the CF parameters of variant I (V.I, Fig. 5).

This set of energies of the CF levels (a number of the others are probably possible) is obtained when using the CF scheme 1:3:2:3 (i.e., when $J = 4$ manifold splits into a singlet Γ_1, a doublet Γ_3, and two triplets Γ_4 and Γ_5), although the radical problem lies here in the assumption of a well-defined number of electrons responsible for an AFM ordering in UN. This shows merely an issue of the possible presence of the U^{+4} ions in UN with the $5f^2$ configuration, with the $^3H_4$ ground multiplet within the framework of a localized 5*f*-electron picture. The earlier papers by de Novion [51] or Lemmer and Lowther [7], who considered the two-level system (singlet-triplet) with an energy separation 210 or 177 K, respectively, accounted for the temperature dependencies of a sublattice magnetization, $m_U(T)$, induced by a molecular field. Moreover, the latter authors, by taking into account the scheme Γ_1,Γ_4,Γ_3, and Γ_5, were able to account for the Curie-Weiss behavior of the average susceptibility $\chi_{av}(T)$ in a broad temperature range, as already mentioned. Moreover, they proposed the above CF scheme with the total spread energy of about $\Delta_{CF} \approx 700(15)$ K. This total energy is not far from our value of 900 or 718 K reported in Ref. [5]. In

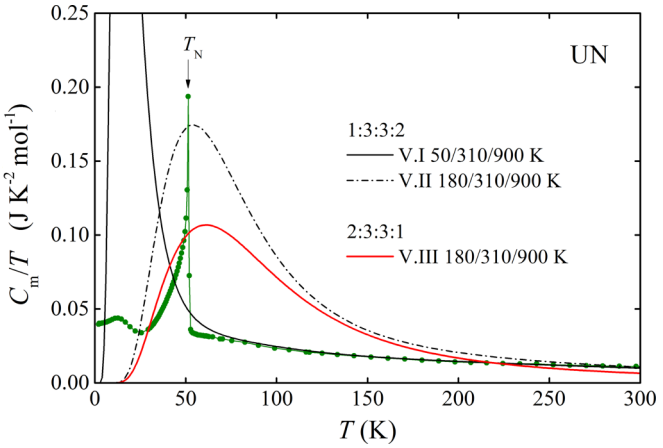

FIG. 5. Magnetic specific heat part of UN divided by temperature, C_m/T vs T. The black solid line represents the best fit of the theoretical Schottky function to the uranium CF scheme V.I 1:3:3:2, while the dot-dashed and red solid lines show the fitting to CF schemes V.II 1:3:3:2 and V.III 2:3:3:1, respectively, where the numbers indicate degeneracy of the particular levels. The corresponding energy differences in relation to the ground state are indicated in the figure. See discussion of Schottky behavior in UN in the main text.

the case of the pure singlet Γ_1, which is a ground state, a conventional Kondo effect is excluded—this effect is absent in the temperature-dependent electrical resistivity $\rho(T)$ above T_N of UN after correction with the phonon contribution [8]. As demonstrated in our previous paper, the observed strong negative curvature of this dependence in the paramagnetic region is characteristic of the CF interaction, with a calculated similar value of separation of the two lowest CF levels (no alternative exists). Similar evidence of the CF influence on the resistivity of UN in the paramagnetic region was also discussed in Ref. [51]. Thus, such behavior of $\rho(T)$ caused by the CF interaction is observed in many Ce compounds, particularly in Ce monopnictides [52]. However, following the discussion given in Ref. [53] for the singlet-triplet system $PrFe_4P_{12}$ that is similar to that of UN, the observed Kondo behavior in this skutterudite was explained by considering f^2/f^3 configuration mixing due to conduction-f-electron hybridization.

Among the strong arguments for a singlet CF ground state in UN there are also those provided by specific heat measurements taken in zero and in magnetic fields. It appears that it is hard to see any field dependence of $\gamma(0)$ in applied magnetic fields up to 3.5 [24] or 9 T (this paper, but not shown), which unveils the nonmagnetic character of the ground state. In particular, zero-field Schottky-like behavior, as shown above, can be related to the Γ_1–$\Gamma_4(\Gamma_5)$ levels, which are the lowest-lying CF states. As is evident from Fig. 5, the Schottky-like anomaly extracted in this paper above T_N cannot be explained if taking into account $\Delta_{12}(\Gamma_1$–$\Gamma_4) \approx 180$ K (Variant II [V.II], Fig. 5). However, there is no doubt that this has to do with the distinct CF splitting of the localized $5f$ states in UN, despite its partial hybridization with other electrons and hence a metallic character of UN. For comparison, in Fig. 5, we display Variant III (V.III), also representing a nonmagnetic ground state, which

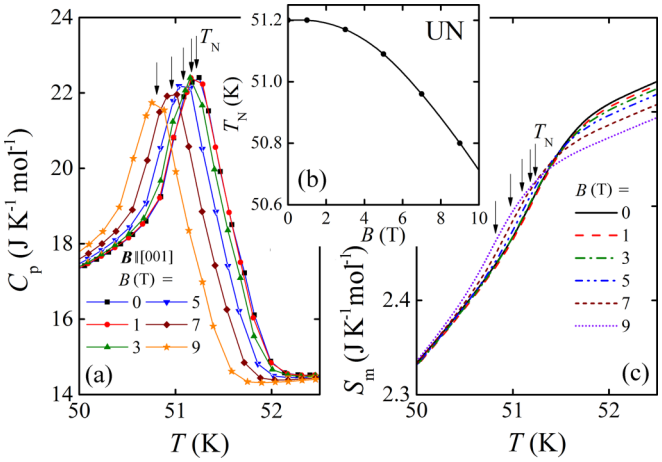

FIG. 6. (a) The specific heat C_p of UN measured in the magnetic field up to 9 T as a function of temperature. (b) The Néel temperature vs magnetic field, taken as a maximum in the C_p vs T functions plotted in (a). (c) The magnetic entropy S_m vs T determined in applied magnetic fields. The arrows mark the Néel temperatures.

is the Γ_3 doublet but is not further discussed because it is considered improbable.

Figure 6 displays the specific heat of UN measured in the region of the phase transitions in magnetic fields up to 9 T applied along the [001] direction. As seen from Fig. 6(a) and (b), there is only a small shift of T_N toward lower temperatures with rising magnetic field strength. Simultaneously, the peaks in $C_p(T)$ taken in several magnetic field strengths become less pronounced, and their widths diminish slightly. Hence, one observes that the magnetic entropy S_m (calculated after subtraction of the phonon contribution) becomes below T_N slightly higher in applied fields than that in the zero field, though the entropy is normally a decreasing function of the magnetic field.

In turn, $S_m(T)$, taken slightly above T_N and further at higher temperatures, becomes relatively lower in the increasing magnetic field compared with that estimated at the zero field [Fig. 6(c)]. Such behavior of $S_m(T)$ is a result of a change in energies between the ground state singlet and the Zeeman splitting of the excited CF levels, as is the case for $PrOs_4Sb_{12}$ [54]. The $S_m(T)$ function of UN reaches at T_N a value of $2.53\,\mathrm{J\,mol^{-1}\,K^{-1}}$, which is relatively far from $Rln2 = 5.76\,\mathrm{J\,mol^{-1}\,K^{-1}}$, when the CF (pseudo)doublet would be the ground state. It appears, however, that using the model presented by Grunzweig-Genossar [55], who assumes the presence of U^{4+} ions, with a singlet ground state Γ_1 and the excited triplet Γ_4, one may explain the value of the magnetic entropy at T_N that is lower than expected from the above doublet. For instance, following Ref. [55], $S_m(T_N)$ can be expressed by Eq. (4):

$$S_m = Nk_B\{\ln[1 + g_2\exp(-x)] + xg_2\exp(-x)/[1 + g_2\exp(-x)]\}. \quad (4)$$

S_m is a function of g_2 (degeneracy of the first excited level) and $x = \Delta_{12}/k_BT_N$ in two-level approximation. In our case of estimated $S_m(T_N)$, we get just the value $x \approx 3.6$, which corresponds to $\Delta_{12} \approx 180\,\mathrm{K}$. Thus, the latter energy separation is in accordance with that proposed from the $m_U(T)$ function, as discussed above. Taking into account a small value of $S_m(T_N)$ ($\approx 0.71\,\mathrm{J\,mol^{-1}\,K^{-1}}$) previously reported by Westrum and Barber [40], where x is close to unity, Δ_{12} is increased up to about 280 K, which is rather unreliable. To explain our fitting value $\Delta_{12} \approx 50\,\mathrm{K}$ (Fig. 5), S_m at T_N based on Eq. (4) would reach such an unrealistically large value as $10.8\,\mathrm{J\,mol^{-1}\,K^{-1}}$, which is close to the quartet ground state ($Rln4 = 11.53\,\mathrm{J\,mol^{-1}\,K^{-1}}$). This situation underlines again that the complex character of UN still requires deeper investigation, which also follows from its physical properties considered below.

B. Low-temperature anomalous properties

1. Specific heat

As shown in the preceding paragraph, there is a distinct anomaly in the $C_p(T)$ curve, in which a diffuse maximum is formed around $T = 12\,\mathrm{K}$ except for a sharp peak observed at T_N, which is reminiscent of a weak first-order transition. On one hand, the low-T maximum starts just below $T^*(\approx T_N/2)$. On the other hand, such small diffuse maxima were also found, but near T^*, in ferromagnets UGe_2 [56] and UCu_2Si_2 [57]. Their presence was interpreted as charge (spin) density wave (C/SDW) fluctuations superimposed on localized FM moment behavior. However, it requires further study in a microscopic scale in order to explain such a type of a coexistence. Below, we analyze other low-temperature anomalies of UN, as those appearing in TEP, electrical resistivity $\rho(T)$, magnetoresistivity ($\Delta\rho/\rho_0$), and ThC.

2. TEP and electrical resistivity

Thermoelectric power for single-crystalline UN was measured in our previous paper [8] along three main crystallographic directions and in a wide temperature range. The $S(T)$ of UN reaches at RT a value as large as $50\,\mu\mathrm{V\,K^{-1}}$, which is comparable to that of UGe_2 ($35\,\mu\mathrm{V\,K^{-1}}$ for $\nabla T||[010]$) [56]. A high value of TEP already recorded at RT originates from a low number of charge carriers. As Hall measurements of a UN single crystal by Kanter [58] showed, the conductivity was done by $Z = 0.876$ electrons per one U atom. Just this value is close to that ($Z = 1$) used in the model presented in Ref. [5], in which the ratio of electron masses m^*/m_e was assumed to be 3.

In general, TEP of UN decreases monotonically with decreasing temperature down to T_N, where it drops sharply and finally goes through a negative minimum at $T^*(\approx T_N/2)$ before approaching $S = 0\,\mu\mathrm{V\,K^{-1}}$ at the lowest temperature. In Fig. 7(a), we present the $S(T)$ low-temperature data of UN taken for the temperature gradient $\nabla T||[100]$ against the reduced temperature scale. Such a negative minimum in $S(T)$ is also often observed for ferromagnets below their T_C's (e.g., UGe_2 along $\nabla T||a$ [56]) or antiferromagnets below their T_N's (e.g., UPdSn and UCuSn [59]), as well as for nonordered magnetically uranium systems (e.g., USn_3, UIr_3, and UPd_3 [60]). The sign change in TEP of UN that takes place in the temperature region 35–40 K, giving rise to a crossover from electronlike to holelike heat carriers, was observed for all three main crystallographic directions [8].

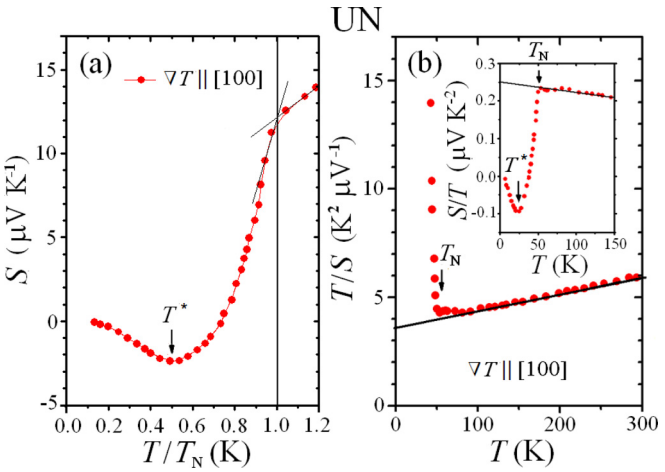

FIG. 7. (a) Thermoelectric power S measured for the gradient $\nabla T||[100]$ against the reduced temperature T/T_N. (b) The ratio T/S vs T function for the gradient $\nabla T||[100]$. Note a straight-line behavior above T_N. The inset demonstrates more distinctly the low-temperature minimum at T^* in the S/T vs T function.

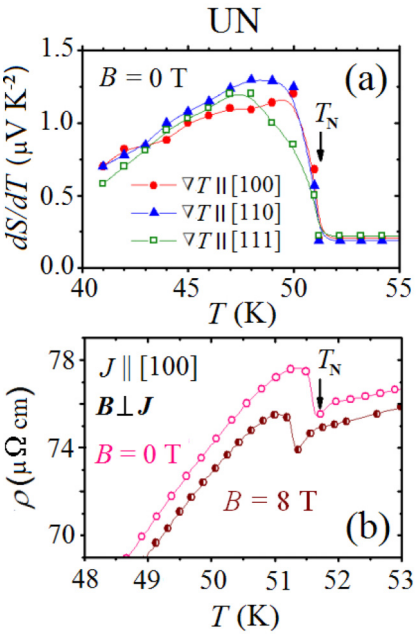

FIG. 8. (a) The dS/dT vs T function around T_N determined for gradient ∇T parallel to three main crystallographic axes. The T_N value is the same as that found from magnetic susceptibility and electrical resistivity [8] or specific heat (this paper). (b) The SDW-like anomaly in the $\rho(T)$ function drawn on an enhanced scale measured in 0 T and a field of 8 T for the current $\boldsymbol{J}||[100]$. For the other main crystallographic axes, see Ref. [8].

As Fig. 7(a) demonstrates, a significant change in the slope of the $S(T/T_N)$ function takes place around T_N. This slope change at the transition is approximately from 0.16 to 1.1 μV K^{-2} when going from the paramagnetic to the AFM region. A similar distinct change in that slope was found for Cr metal [61]; however, this can be regarded as a mirrorlike reflection of that in UN around the T/T_N axis. Furthermore, in Fig. 7(b), we have plotted the T/S vs T dependence taken for the same temperature gradient direction as above. As seen, this dependence is a straight line in the wide temperature range T_N–300 K. It means that the high-temperature region of $S(T)$ where $T > T_N$ can be described by the phenomenologically derived function $S(T) = AT/(1 + T/T')$, where T' is the characteristic temperature. The parameters are as follows: $A = 0.28\,\mu$V K^{-2} and $T' = 450$ K. These parameters may be compared, e.g., to those found for UNi_2Al_3($A = 0.24\,\mu$V K^{-2}, $T' = 250$ K [62]). The characteristic temperature T' is regarded as being scaled with the temperature of the maximum resistivity and has some tendency to saturation. Such a dependence is also obeyed for UPd_2Al_3, UBe_{13}, UPt_3, and $UCu_{4+x}Al_{8-x}$ systems (see Ref. [62]). In the inset to Fig. 7(b), we display also the S/T vs T function for UN with the heat current along [100]. The value of S/T at $T = 0$ K is 0.25 μV K^{-2}. Taking this value together with that of $\gamma(0)$ (=45 mJ mol^{-1} K^{-2}), as found in this paper, one can calculate a dimensionless ratio $q = (S/T)[N_{Av}e/\gamma(0)]$, which links the Seebeck coefficient to the electronic specific heat through the Faraday number $N_{Av}e(\approx 10^6$ C mol$^{-1})$ [63]. For UN, this ratio is about 0.5 and can be compared to those reported in Ref. [62] for UNi_2Al_3 (0.2) and UPd_2Al_3 (0.3). For a range of strongly interacting electronic systems, this ratio is close to unity in the $T = 0$ limit despite the systems' various band structures.

Furthermore, it is interesting to compare for UN the temperature dependence of the Seebeck coefficient and the electrical resistivity, both of which are in the critical region of the paramagnetic-to-AFM transition. Therefore, we have plotted in Fig. 8(a) dS/dT as a function of temperature. In this figure, one observes for all three heat current directions that an almost isotropic bump in the behavior of this function is formed just below T_N.

In Fig. 8(b), we demonstrate an appearance of a small hump formed in the electrical resistivity of UN just below T_N, which already has been mentioned in this paper (see also Ref. [8]). We present this hump on the enhanced scale taken at 0 and 8 T, but only for the current $\boldsymbol{J}$ applied along the [100] direction. This Cr-like anomaly may indicate the formation of an SDW gap in the FS because of the nesting, as visualized in Fig. 1(a). In the two magnetic subsystems involving the 5f electrons, as we propose here for UN, we deal with (1) local CF split moments on the U^{4+} sites and (2) conduction electrons exhibiting the nested FS (Fig. 1). Therefore, one can assume that electron-electron interaction causes an SDW transition in the nested parts of the FS, which coexists with the induced local ordered state. Such coexistence requires common acceptance by researchers and an extended microscopic investigation not only for UN but also for many other uranium compounds that are magnetically ordered. Up to now, the literature has offered a number of cases similar to UN, especially when the specimen is an antiferromagnet at low temperatures. We present here the one example, namely, tetragonal $UNiGa_5$, cited in the literature as having SDW behavior with $T_N = 85$ K and $\gamma(0) = 30$ mJ mol^{-1} K^{-2} [64,65]. For both these compounds, i.e., UN and $UNiGa_5$, one observes a similar respond to applied pressure. For example, the Néel temperatures for UN [66] and $UNiGa_5$ [67] decrease smoothly under pressure, and the resistivity humps first become broader and finally vanish

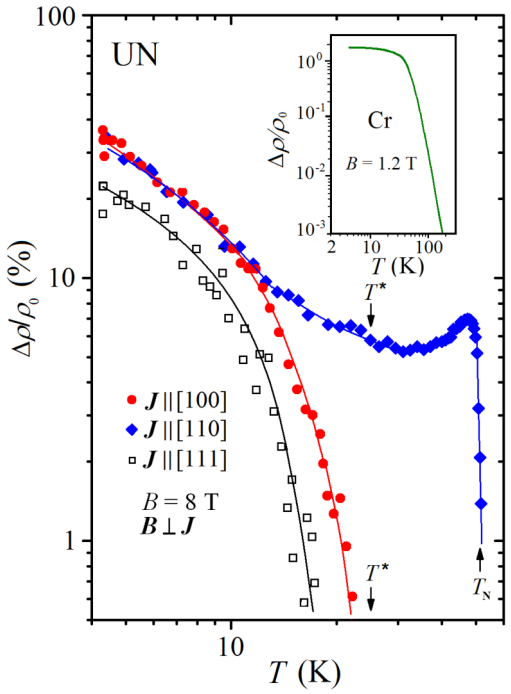

FIG. 9. Magnetoresistivity $\Delta\rho/\rho_0$ against temperature T for UN measured along the three main crystallographic axes in the log-log scale compared to that reported for Cr [70] (see the inset). The $\Delta\rho/\rho_0(T)$ for $\boldsymbol{J}||[110]$ changes with the temperature quite differently from those for $\boldsymbol{J}||[100]$ and $J||[111]$ above 10 K. For $\boldsymbol{J}||[110]$, a hump occurs just before reaching T_N.

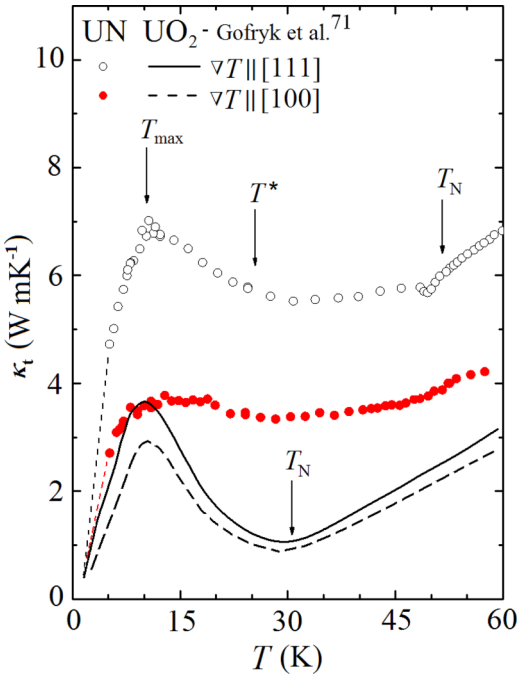

FIG. 10. The ThC κ_t of UN as a function of temperature measured along two main crystallographic directions, namely, when the temperature gradient is applied parallel to [100] or [111] directions. The large anisotropy in the $\kappa_t(T)$ functions observed in the paramagnetic, as well as AFM, states is unexpected for a cubic unit cell. Similar anisotropy has been recently pointed out by Gofryk *et al.* [71] for the cubic UO_2 The arrows show anomalies at the characteristic temperatures described in the text. Both UN and UO_2 systems exhibit this similar thermal behavior at low temperature.

before reaching the critical pressure p_c (where $T_N = 0$ K), estimated as 3.5 and 4.5 GPa, respectively. Despite the low value of the effective magnetic moment of uranium deduced for the latter gallide, Kato *et al.* [68], based on Knight shift vs susceptibility measurements, have concluded that the uranium f electrons participate in the formation of both the conduction band and the localized moments. One can infer the same behavior from the nuclear magnetic resonance (NMR) of ^{14}N papers on UN by Kuznietz [69].

In Fig. 9, we display the transverse magnetoresistivity (TMR) of UN, defined as $\Delta\rho/\rho_0 = [\rho(H) - \rho(0)]/\rho(0)(\%)$, in the log-log scales measured for $\boldsymbol{J}$ along the three main crystallographic axes. As seen, $\Delta\rho/\rho_0$ for all three directions is positive in the region of low temperatures, where TMR reaches high values varying between 23 and 36% at 4.2 K, depending on the current direction. It appears that their temperature dependencies (for $J||[110]$ only up to 10 K) are reminiscent of that of Cr [70] (see the inset). This is also the case for UGe_2 [56], which exhibits a similar hump in $\rho(T)$ just below the Curie temperature but only for $J||[010]$. As pointed out in Ref. [8], TMR of UN for the current $J||[100]$ and [111] changes its sign around T^* (marked in Fig. 9) and becomes slightly negative above this characteristic temperature due to either a weak Kondo-like interaction or magnetic fluctuations.

3. *Thermal conductivity*

In Fig. 10, we display the low-temperature ThC, κ_t, of UN taken for the temperature gradient applied along two crystallographic directions, i.e., [100] and [111]. From this figure, the $\kappa_t(T)$ function of UN is substantially anisotropic—especially in the paramagnetic state, where its crystal structure is fully cubic (see also Ref. [8]). Thus, for materials with a cubic symmetry, ThC should be isotropic [71].

Perhaps a very small tetragonal distortion of the NaCl-type structure of UN in the AFM state [15] could justify some of the anisotropic behavior of ThC below T_N. However, any distinct difference with respect to the paramagnetic state is only seen in the region of the maximum in $\kappa_t(T)$ occurring about $T_{max} = 10$ K. It is apparent that there is some correspondence between this maximum and that detected in the low-temperature magnetic specific heat, also formed just below T^* (Fig. 4). The ThC maximum arising at low temperature has its origin in a rapid increase of electron-phonon scattering just below T_N rather than in the phonon-phonon scattering. A large resemblance to the low-temperature $\kappa_t(T)$ behavior of UGe_2 also exists, even though it is a ferromagnet [72]. However, the latter maximum appears exactly at T^*. The Néel temperature is weakly marked on $\kappa_t(T)$ by a shoulder for both measured directions, again as is the case near the Curie temperature of UGe_2. For the sake of comparison in Fig. 10, we have plotted the same data found for a UO_2 single crystal that has cubic symmetry [71], which also exhibits ThC anisotropy. The authors of Ref. [71] are trying to explain such an unexpected fact by breaking cubic symmetry due to coupling to the applied temperature gradient. The ThC of UN becomes dominated by the electronic part only at higher temperatures,

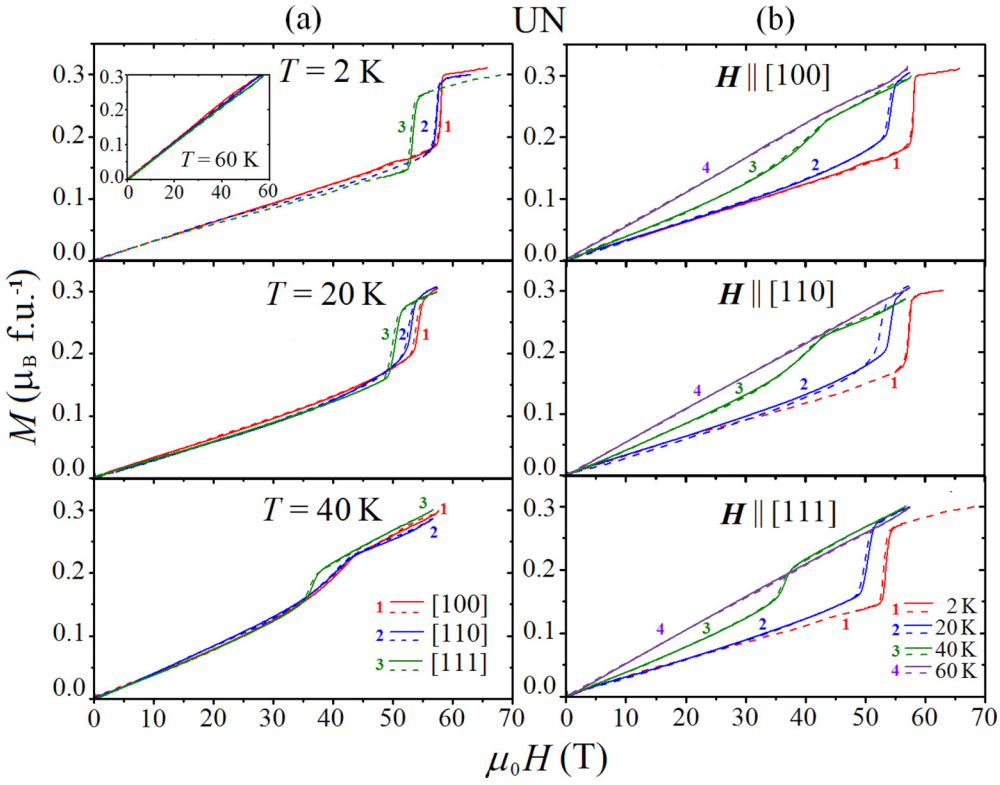

FIG. 11. (a) Magnetization curves M vs $\mu_0 H$ for the three main crystallographic directions taken at 2, 20, 40, and 60 K. (b) Magnetization curves M vs $\mu_0 H$ taken for the indicated temperatures for the particular crystallographic axes. If a hysteresis in the magnetization curves takes place, it is of the order of 1 T, which is difficult to be observed. Nevertheless, it is supposed that the high-field transitions observed in UN are first-order ones.

while the phonon scattering decreases rapidly with increasing temperature, as visualized in Ref. [73] by showing the existing relation between UN and UO_2 in their high-temperature $\kappa_t(T)$ behavior. Almost spherical valence charge densities near U and N atoms in the UN (001) plane were revealed by Long *et al.* [74], indicating high-level iconicity of UN, which is similar to that of UO_2.

4. High-field studies

The magnetic phase diagram of UN has not been known up to now in the H-T plane in spite of its importance in understanding the nature of magnetic ordering because the values of the critical fields of metamagnetic transitions provide information on the strength of the exchange interaction between the antiparallel-coupled FM sheets (001). We deal here with three types of equivalent domains; hence, the FM sheets are also parallel to (100) or (010) ones. The first step in this direction was made almost four decades ago by magnetization measurements of the polycrystalline UN up to 35 T [1]. The result of this paper was rather unexpected due to the lack of a metamagnetic transition even in such a high applied field, while other uranium monopnictides, like isostructural UP or UAs, have just such a type of transition in considerably lower values of critical field strengths $\mathbf{B}_{cr}$ [1].

In this paper, we present the high-field data of magnetization studies made up to 65 T on the single-crystalline samples of UN, which are cut along the three main crystallographic directions from the same ingot as those specimens used in other bulk studies here. The results of these studies are given in Figs. 11–13. In Fig. 11(a), we show the magnetization M vs B (or $\mu_0 H$) measured along the three axes, [100], [110], and [111], and taken at four temperatures: 2, 20, 40, and 60 K. In Fig. 11(b), we also present the variations of M where the magnetic field is applied parallel to the particular crystallographic directions and temperatures are kept as given above.

Now, it is clear that a sharp metamagnetic transition occurs in UN when, e.g., $\mathbf{B}_{cr}$ reaches at 2 K a high field such as 58 T for H||[100]. From this figure, one can see some differences in the values of $\mathbf{B}_{cr}$, depending on the given axis of measurements. For temperatures 2, 20, and 40 K, we have $\mathbf{B}_{cr}[100] \approx \mathbf{B}_{cr}[110] > \mathbf{B}_{cr}[111]$, while at 60 K, when UN is in the paramagnetic state, all three magnetization curves form almost one straight line (i.e., there is a lack of apparent anisotropy). It was further found that $\mathbf{B}_{cr}$ for all three directions follows the function $\mu_0 H_{cr}(\mathrm{T}) = \mu_0 H_{cr}(0) - kT^2$, where the coefficient $k \approx 0.01\,(\mathrm{T\,K^{-2}})$ [Fig. 12(a)]. This function gives 76 K at $\mu_0 H_{cr} = 0$ while $T_N = 51.2$ K. It means that near this critical temperature where $\mu_0 H_{cr}$ reaches a value of about 30 T, the critical fields drop abruptly to zero at T_N, as is the case for tetragonal URu_2Si_2, for which three-step metamagnetic transitions, occurring along the c axis, were reported [75]. We compare our results to those obtained for this silicide, because a number of papers (see Ref. [76] and references therein) present this compound as having the CF singlet as a ground state.

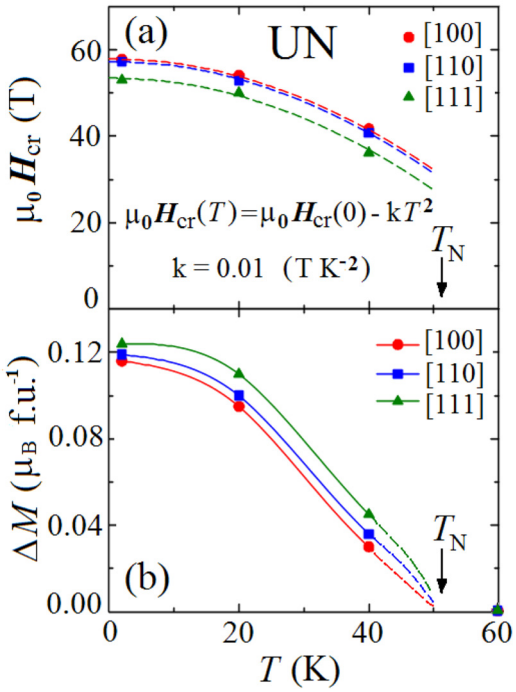

FIG. 12. (a) Temperature variations of $\mu_0 H_{cr}$ for the three main crystallographic directions. There must have been a jump at the critical field down to zero as the temperature reaches T_N. (b) Temperature variations of the magnetization jump ΔM determined for the three crystallographic directions. Both types of curves indicate how large anisotropy is in the critical fields and the moment jump orientation of the UN crystals depending on their relation to the applied magnetic field.

As we will point out below, the difference between UN and URu_2Si_2 is that for the latter compound, an applied field up to 60 T was sufficient to obtain full magnetization in its three-step manner, whereas for UN, we observe only one jump in magnetization, with $\Delta M \approx 0.12\mu_B$ at 2 K. In Fig. 12(b), we demonstrate how ΔM changes with temperature measured for all three crystallographic directions, assuming that $\Delta M = 0$ at T_N. Next, taking into account a full value of the ordered moment of $0.75\mu_B$ for UN [6], one finds that among 12 atomic layers, only 1 layer of moments is reversed under the field forming an induced ferrimagnetic state, which results in $\Delta M = 0.75 \times 2/12 \approx 0.12\,\mu_B$.

To reproduce the H-T diagram of UN and to estimate the zero-temperature field of the transition to the paramagnetic phase, we consider a layer model of the Ising spins. The relevant Hamiltonian reads

$$H = -\sum_n \left(J \sum_{i,j} S_i^n S_j^n + \sum_{\alpha=1}^{6} J_\alpha \sum S_i^n S_j^{n+\alpha} \right) \quad (5)$$

where $S_i{}^n$ denotes an Ising spin $S = \pm 1$, i numbers spins in the plane, and n numbers planes. In order to describe the phases AFM($+-+-$), ferrimagnetic $f12$($+-+-+-+-+-++$), FM($++++$) experimentally observed in UN, and ferrimagnetic $f6$($+-+-+++-+-++$), which could be realized for the symmetry reason, one should consider at least 12 layers. We confine ourselves to nearest-neighbor coupling in the plane and the sixth order between planes. Introducing denotations

$$R_1 = J_1 + J_3 + J_5, \quad R_2 = J_2 + J_4 + J_6 \quad (6)$$

and comparing the ground state energies of the states AFM, $f12$, $f6$, and FM, one gets for $R_1 < 0, R_2 < 0$ and

$$J_6 < 3R_2/5 \quad (7)$$

the following sequence of the phases with increasing field:

$$\text{AFM} \rightarrow f12 \rightarrow \text{FM}. \quad (8)$$

For

$$0 > J_6 > 3R_2/5, \quad (9)$$

the additional phase $f6$ appears, and one should observe the sequence AFM $\rightarrow f12 \rightarrow f6 \rightarrow$ ferromagnetic, whereas for $J_6 > 0$, there is a direct transition from AFM to $f6$ and then to FM.

In the simplest version of the molecular field approximation (MFA), Néel temperature T_N is given by

$$T_N = -2(R_1 - R_2 - J), \quad (10)$$

and the paramagnetic Curie temperature

$$\theta_p = 2(R_1 + R_2 + J). \quad (11)$$

Assuming that $J_6 < 0$, the zero-temperature transition field H_{AFM} from the AFM to the $f12$ phase is given by

$$H_{AFM} = -2(R_1 - R_2). \quad (12)$$

Knowing the experimentally found values of Néel temperature $T_N = 51.5\,\text{K}/0.67 \approx 77\,\text{K}$, paramagnetic Curie temperature $\theta_p = -249\,\text{K}/0.67 \approx -372\,\text{K}$, and approximated to the $T = 0$ field $H_{AFM} = 57\,\text{T}$, one can roughly estimate the couplings J, R_1, and R_2:

$$\begin{aligned} 57 &= -2R_1 + 2R_2, \\ 77 &= -2R_1 + 2R_2 + 2J, \\ -186 &= J + R_1 + R_2. \end{aligned} \quad (13)$$

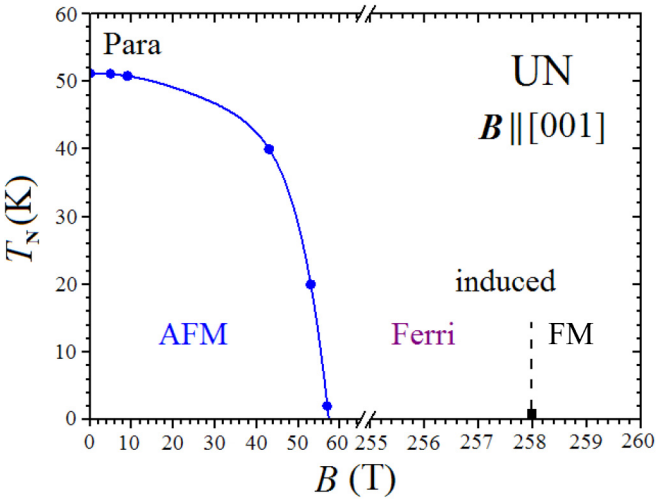

FIG. 13. Magnetic phase diagram of UN. Notice the breaking of the field scale and the theoretical point of 258 T, where above such a high field one could await full magnetization of all moments along the one direction (induced ferromagnetism).

This yields $R_1 \approx -112, R_2 \approx -84$, and $J \approx 10$. If the system realizes the scenario in Eq. (8), $J_6 < 3R_2/5$, one can calculate the value of the zero-temperature transition field H_{FM} between the $f12$ and the FM phases using the following formula:

$$H_{\mathrm{FM}} = -2R_1 - 2R_2/5 \approx 258\,\mathrm{T} \tag{14}$$

If $J_6 > 3R_2/5$, to find the transition field to the induced FM phase, one needs additional measurements that allow estimation of the coupling J_6. Taking into account the values of the critical temperatures for transitions from AFM to paramagnetic or AFM to ferrimagnetic based on our either specific heat measurements in low magnetic fields or those in high magnetic fields, respectively, we present the magnetic phase diagram of UN in Fig. 13. In addition, we put a supposed limit of the critical field for the induced transition from ferrimagnetic to FM based on our rather simple calculations. Therefore, the value 258 T has only a demonstrative aspect of how strong magnetic fields should be used to reverse all FM layers in the parallel arrangement and obtain the full magnetization of $0.75\mu_{\mathrm{B}}$.

V. SUMMARY AND CONCLUSIONS

Detailed analysis of the magnetic contribution to the specific heat of single-crystalline UN showed that it exhibits two distinct anomalies: a sharp one at T_{N} associated with large magnetic entropy, characteristic of a long-range AFM order of localized magnetic moments, and a broad one starting below $T^* = T_{\mathrm{N}}/2$ accompanied by much smaller entropy, which can be ascribed to the presence of an SDW-like transition. Our analysis also revealed the presence of a Kondo-like interaction and CF effect in UN. Furthermore, the specific heat measurements showed low sensitivity of the T_{N} transition to the magnetic field up to 9 T. The high-field magnetization measurements yielded at 2 K the field-induced metamagnetic phase transition at 58 T, which diminished rapidly with increasing temperature. The latter behavior of UN allowed us to construct a preliminary magnetic phase diagram, which was easily reproduced by considering a layer model of the Ising spins. This model predicted a transition to the fully field-induced ferromagnetism at as high a field as 258 T. In addition, we have analyzed our calculated FS and results of transport property measurements, performed for this compound, aiming to show the similarity of its behavior and Cr-like SDW behavior. All these showed some deviations from purely itinerant or purely localized behavior. As a consequence, we consider here the dual model for UN.

The question of whether the $5f$ electrons are localized or itinerant in actinide compounds had been a key topic for many decades before the beginning of 2000, when the above idea found a strong support in theoretical undertakings. Earlier, it was difficult to interpret, e.g., the coexistence of strong magnetism and superconductivity by unified look, as was the case for two exemplary systems: AFM UPd_2Al_3 and FM UGe_2 (see the review in Ref. [78]). However, one thing was unquestionable: both phenomena unveiled in these compounds had the $5f$-electron origin. In the text, we have mentioned building a theoretical foundation of that problem (see Ref. [23]). Furthermore, based on many experimental measurements, it was found for those illustrative compounds that the above coexistence behaves as arising from two different, separated substates of the $5f$ electrons: localized and itinerant. For instance, see the results of muon-spin rotation (μsR) measurements for UPd_2Al_3 [79] and UGe_2 [80]. However, the idea of two substates in a $5f$ system (which originated in 1990) was based on just such measurements of UCu_5 [81]. The AFM behavior of the latter compound seems to be reminiscent of that in UN. Previously, we also yielded more experimental and theoretical arguments about $5f$ dualism, not only for uranium digermanide [56] but also for another system, such as UCu_2Si_2 [57], even though this FM silicide, as well as AFM UCu_5 and UN, does not exhibit superconductivity down to 2 K. Moreover, we have argued for the dual model in the case of UFe_2Al_{10}, which is a magnetically nonordered uranium compound to the lowest temperatures [82].

The main purpose of our paper on UN was to unveil numerous peculiar behaviors reported in the past [8] and the new ones presented here, which together supposedly reflect the dual nature of the $5f$ electrons in UN and are in contrast to a common opinion that all $5f$ electrons in this mononitride are itinerant. The latter thesis has been underlined by papers by Fujimori *et al.* [10,77]. It would be desirable to continue studying this model compound by applying a number of outstanding experimental methods that allow for the explanation of controversial statements by at least using pure single crystals such as those we used in previous and the present papers. It is puzzling that from the time of the first magnetic studies of UN [1] (about 55 years ago), there has been a lack in the literature of investigations like de Haas–van Alphen (dHvA) or Shubnikov–de Haas (SdH) oscillations but especially TEP oscillations. The latter measurements of quantum oscillations in UGe_2, by using TEP [83], allowed verification of the FS of this low-symmetry ferromagnet. Compton scattering profiles or two-dimensional angular correlations of positron annihilation radiation (2D ACAR) are also desirable in studies of the FS of this mononitride even at elevated temperatures. The latter are particularly relevant for probing strongly correlated electron materials such as UGe_2 (see, e.g., Ref. [84]). Most useful could be investigations of the electronic structure of UN by ultrafast optical spectroscopy (UOS). For example, an analysis of such data made for antiferromagnet USb_2 [85] indicated a gap caused by hybridization between localized $5f$ electrons and conduction electrons, while the band renormalization involving magnons was responsible for the appearance of another gap. Furthermore, one would wish to have detailed data of resonant x-ray magnetic scattering (RXMS) and x-ray magnetic circular dichroism (XMCD). Again, the single-crystalline UGe_2 examined by these types of measurements sheds light on its dual electronic behavior [86,87]. However, the most important proofs of the coexistence of two electronic substates in UN or UGe_2 are based on neutron diffraction studies underlining the ionic (U^{4+}) character of their form factors [6,88]. This gives evidence that the observed magnetic order is certainly of the localized character. Instead, in the literature, the magnetic orders in UN or UGe_2 are presented as itinerant. Moreover, the numerous band structure calculation results, as commonly published, are unable to explain all aspects of this mononitride that are discussed in this paper, e.g., crystal field effects of nearly localized electron states.

ACKNOWLEDGMENTS

We thank P. de V. Du Plessis for supplying the UN single crystals, E. Talik for making analyses of the stoichiometry and purity of the used crystals, and C. Sułkowski for providing measurements of the thermoelectric data around the critical region. The paper was supported by Project No. 16-03593S of the Czech Science Foundation and the program of Czech Research Infrastructures (Project No. LM2011025). We acknowledge the support of Hochfeld-Magnetlabor Dresden (HLD) at Helmholtz-Zentrum Drezden-Rossendorf (HZDR), a member of the European Magnetic Field Laboratory (EMFL). The Computing Center at the Institute of Low Temperature and Structure Research of the Polish Academy of Sciences in Wrocław is acknowledged for use of the supercomputers and technical support.

[1] R. Troć, in *Landolt-Börnstein Numerical Data and Functional Relationship in Science and Technology*, New Series, Group III: Condensed Matter, edited by H. P. J. Wijn (Springer-Verlag, Berlin, 2006), Vol. 27-B,6α, p. 491.
[2] C. F. Van Doorn and P. de V. Du Plessis, J. Low Temp. Phys. **28**, 391 (1977).
[3] K. Kubo and T. Hotta, J. Phys. Soc. Jpn. **75**, 013702 (2006).
[4] G. H. Lander, D. J. Lam, J. F. Reddy, and M. H. Miller, AIP Conf. Proc. No. **18**, 442 (1974).
[5] J. Grunzweig-Genossar, M. Kuznietz, and F. Friedman, Phys. Rev. **173**, 562 (1968).
[6] N. A. Curry, Proc. Phys. Soc. London **86**, 1193 (1965).
[7] R. H. Lemmer and J. E. Lowther, J. Phys. C Solid State Phys. **11**, 1145 (1978).
[8] M. Samsel-Czekała, E. Talik, P. de V. Du Plessis, R. Troć, H. Misiorek, and C. Sułkowski, Phys. Rev. B **76**, 144426 (2007).
[9] T. M. Holden, W. J. L. Buyers, E. C. Svensson, and G. H. Lander, Phys. Rev. B **30**, 114 (1984).
[10] S.-i. Fujimori, T. Ohkochi, T. Okane, Y. Saitoh, A. Fujimori, H. Yamagami, Y. Haga, E. Yamamoto, and Y. Ōnuki. Phys. Rev. B **86**, 235108 (2012) and references therein.
[11] J. M. Fournier, J. Beille, A. Boeuf, C. Vettier, and A. Wedgwood, Phys. **102B**, 282 (1980).
[12] R. Troć, J. Solid State Chem. **15**, 14 (1975).
[13] T. M. Holden, W. J. L. Buyers, E. C. Svensson, and G. H. Lander, Phys. Rev. B **26**, 6227 (1982).
[14] H. H. Hill, in *Plutonium and Other Actinides,* edited by W. N. Miner (Metal Society AIME, New York, 1970), p. 2.
[15] R. C. Maglic, G. H. Lander, M. H. Mueller, and R. Kleb, Phys. Rev. B **17**, 308 (1978).
[16] R. Troć, W. Trzebiatowski, and K. Piprek, Bull. Acad. Polon. Sci. Ser. Sci. Chim. **19**, 427 (1971); R. Troć, R. Wawryk, A. Pikul, and N. Shitsevalova, Phil. Mag. **95**, 2343 (2015).
[17] T. Gouder, R. Eloirdi, F. Wastin, E. Colineau, J. Rebizant, D. Kolberg, and F. Huber, Phys. Rev. B **70**, 235108 (2004).
[18] *Multipak Software Version 6* (Physical Electronics, Eden Prairie, MN, 1998).
[19] Y. Skourski, M. D. Kuz'min, K. P. Skokov, A. V. Andreev, and J. Wosnitza, Phys. Rev. B **83**, 214420 (2011).
[20] P. F. Weck, E. Kim, N. Balakrishnan, F. Poineau, C. B. Yeamans, and K. R. Czerwinski, Chem. Phys. Lett. **443**, 82 (2007).
[21] R. Atta-Fynn and A. K. Ray, Phys. Rev. B **76**, 115101 (2007).
[22] D. Gryaznov, E. Heifets, and E. Kotomin, Phys. Chem. Chem. Phys. **14**, 4482 (2012).
[23] G. Zwicknagl, A. N. Yaresko, and P. Fulde, Phys. Rev. B **65**, 081103(R) (2002); G. Zwicknagl and P. Fulde, J. Phys.: Condens. Matter **15**, S1911 (2003); F. Pollmann and G. Zwicknagl, Phys. Rev. B **73**, 035121 (2006); G. Zwicknagl and M. Reese, J. Magn. Magn. Mat. **310**, 201 (2007).
[24] J. O. Scarbrough, H. L. Davis, W. Fulkerson, and J. O. Betterton Jr., Phys. Rev. **176**, 666 (1968).
[25] T. Ito, H. Kumigashira, S. Souma, T. Takahashi, and T. Suzuki, J. Magn. Magn. Mater. **226-230**, 68 (2001).
[26] T. Durakiewicz (private communication).
[27] P. R. Norton, R. L. Tapping, D. K. Creber, and W. J. L. Buyers, Phys. Rev. B **21**, 2572 (1980).
[28] L. Petit, A. Svane, Z. Szotek, W. M. Temmerman, and G. M. Stocks, Phys. Rev. B **80**, 045124 (2009).
[29] Q. Yin, A. Kutepov, K. Haule, G. Kotliar, S. Y. Savrasov, and W. E. Pickett, Phys. Rev. B **84**, 195111 (2011).
[30] W. Sun, I. Di Marco, and P. Korzhavyi, Mater. Res. Soc. Symp. Proc.1683 **1683**, mrss14-1683-s01-02 (2014).
[31] L. Petit, A. Svane, W. M. Temmerman, and Z. Szotek, Phys. Rev. Lett. **88**, 216403 (2002).
[32] B. Reihl, G. Hollinger, and F. J. Himpsel, Phys. Rev. B **28**, 1490 (1983).
[33] H. Kumigashira, T. Ito, A. Ashihara, H.-D. Kim, H. Aoki, T. Suzuki, H. Yamagami, T. Takahashi, and A. Ochiai, Phys. Rev. B **61**, 15707 (2000).
[34] J. Schoenes, J. Chem. Soc. Faraday Trans. **83**, 1205 (1987).
[35] L. Black, F. Miserque, T. Gouder, L. Havela, J. Rebizant, and F. Wastin, J. Alloy. Compd. **315**, 36 (2001).
[36] K. Koepernik and H. Eschrig, Phys. Rev. B **59**, 1743 (1999); FPLO-5.00-18, http://www.FPLO.de
[37] J. P. Perdew and Y. Wang, Phys. Rev. B **45**, 13244 (1992).
[38] C. F. van Doorn and P. de V. Du Plesis, J. Low Temp. Phys. **28**, 401 (1977).
[39] S. Nasu, T. Kurasawa, H. Matsui, M. Tamaki, and M. Okuda, in *Plutonium and Other Actinides,* edited by H. Blank and R. Lindner (North Holland Publishing, Amsterdam, 1976), p. 515.
[40] E. F. Westrum, Jr. and C. M. Barber, J. Chem. Phys. **45**, 635 (1966).
[41] M. Yoshizawa and T. Suzuki, J. Magn. Magn. Mat. **90-91**, 523 (1990).
[42] M. D. Salleh, J. E. MacDonald, G. A. Saunders, and P. de V. Du Plessis, J. Mat. Science **21**, 2577 (1986).
[43] A. Padel and C. H. de Novion, J. Nucl. Mat. **33**, 40 (1969).
[44] J. Danan, C. H. de Novion, and H. Dallaports, Solid State Comm. **10**, 775 (1972).
[45] F. A. Wedgwood, J. Phys. C **7**, 3203 (1974).
[46] A. A. Aczel, G. E. Granroth, G. J. MacDougall, W. J. L. Buyers, D. I. Abernathy, G. D. Samolyuk, G. M. Stock, and S. E. Nagler, Nat. Comm. **13**, 1124 (2012).
[47] J. Y. Y. Lin, A. A. Aczel, D. L. Abernathy, S. E. Nagler, W. J. L. Buyers, and G. E. Granroth, Phys. Rev. B **89**, 144302 (2014).
[48] E. S. R. Gopal, in *Specific Heats at Low Temperatures* (Plenum Press, New York, 1966).

[49] C. D. Bredl, F. Steglich, and D. Schotte, Z. Phys. B **29**, 327 (2012).
[50] D. A. Joshi, C. V. Tommy, and S. K. Malik, J. Phys.: Condens. Matter **19**, 136216 (2007).
[51] C. H. de Novion, J. Acad. Sci. Paris, Série B **273**, 26 (1971).
[52] See e.g., T. Tsuchida, M. Kawai, and Y. Nakamura, J. Phys. Soc. Jpn. **28**, 528 (1970).
[53] A. Yamasaki, S. Imada, A. Sekiyama, M. Tsunekawa, C. Dallera, L. Braicovich, T.-L. Lee, H. Sugawara, H. Sato, R. Settai, Y. Ōnuki, and S. Suga, J. Phys. Soc. Jpn. **74**, 2045 (2005).
[54] T. Tayama, T. Sakakibara, H. Sugawara, Y. Aoki, and H. Sato, J. Phys. Soc. Jpn. **72**, 1516 (2003).
[55] J. Grunzweig-Genossar, Solid State Comm. **8**, 1673 (1970).
[56] R. Troć, Z. Gajek, and A. Pikul, Phys. Rev. B **86**, 224403 (2012).
[57] R. Troć, Z. Gajek, A. Pikul, H. Misiorek, E. Colineau, and F. Wastin, Phys. Rev. B **88**, 024416 (2013).
[58] M. A. Kanter, Bull. Am. Phys. Soc. **13**, 125 (1968).
[59] H. Kawanaka, H. Nakotte, E. Brück, K. Prokeŝ, N. H. Kim-Ngan, T. Takabatake, H. Fujii, and J. Sakuray, Phys. B **237-238**, 226 (1997).
[60] H. Sato, I. Sakamoto, T. T. Fukuhara, Y. Ōnuki, and T. Komatsubara, J. Phys. Soc. Jpn. **59**, 3687 (1990).
[61] J. B. Sousa, R. S. Pinto, M. M. Amado, J. M. Moreira, M. E. Braga, M. Ausloos, and I. Balberg, Solid State Comm. **31**, 209 (1979).
[62] A. Grauel, D. Fromm, C. Geibel, F. Steglich, N. Sato, and T. Komatsubara, Int. J. Modern. Phys. B **7**, 50 (1993).
[63] K. Behnia, D. Jaccard, and J. Flouquet, J. Phys.: Condens. Matter **16**, 5187 (2004).
[64] E. E. M. Chia, J. X. Zhu, H. J. Lee, N. Hur, N. O. Moreno, E. D. Bauer, T. Durakiewicz, R. D. Averitt, J. L. Sarrao, and A. J. Taylor, Phys. Rev. B **74**, 140409 (2006).
[65] Y. Tokiwa, Y. Haga, E. Yamamoto, D. Aoki, N. Watanabe, R. Settai, T. Inoue, K. Kindo, H. Harima, and Y. Ōnuki, J. Phys. Soc. Jpn. **70**, 1744 (2001).
[66] M. Nakashima, Y. Haga, E. Yamamoto, Y. Tokiwa, M. Hedo, Y. Uwatoko, R. Settai, and Y. Ōnuki, J. Phys.: Condens. Matter **15**, S2007 (2003).
[67] M. Nakashima, Y. Haga, V. Nakawaki, Y. Haga, Y. Uwatoko, R. Settai, and Y. Ōnuki, J. Nucl. Sci. Technol. **39** (Suppl), 214 (2002).
[68] H. Kato, H. Sakai, Y. Tokunaga, Y. Tokiwa, S. Ikeda, Y. Ōnuki, S. Kambe, and R. Walstedt, J. Phys. Soc. Jpn. **72**, 2357 (2003).
[69] M. Kuznietz, Phys. Rev. **180**, 476 (1960).
[70] S. Arajs and G. R. Dunmyre, J. Appl. Phys. **36**, 3555 (1965).
[71] See e.g., K. Gofryk, S. Du, C. R. Stanek, J. C. Lashley, X.-Y. Liu, R. K. Schulze, J. L. Smith, D. J. Safarik, D. D. Byler, K. J. McClellan, B. P. Uberuaga, B. L. Scott, and D. A. Anderson, Nat. Comm. **5**, 4551 (2014).
[72] H. Misiorek, J. Mucha, R. Troć, and B. Coqblin, J. Phys. Condens. Matter **17**, 679 (2005).
[73] J. A. Webb and I. Charit, J. Nucl. Mater. **427**, 87 (2012).
[74] Z. Long, L. Luo, Y. Lu, Y. Hu, K. Liu, and X. Lei, J. Alloys Compd. **664**, 745 (2016).
[75] K. Sugiyama, H. Fuke, K. Kindo, K. Shimohata, A. A. Menovsky, J. Mydosh, and M. Date, J. Phys. Soc. Jpn. **59**, 3331 (1990).
[76] See e.g., V. P. Mineev and M. E. Zhitomirsky, Phys. Rev. B **72**, 014432 (2005); P. Santini, *ibid.* **57**, 5191 (1998).
[77] S. Fujimori, Y. Takeda, T. Okane, Y. Saitoh, A. Fujimori, H. Yamagami, Y. Haga, E. Yamamoto, and Y. Ōnuki, J. Phys. Soc. Jpn. **85**, 062001 (2016).
[78] P. Thalmeyer and G. Zwicknagl, in *Handbook on the Physics and Chemistry of Rare Earths*, edited by K. A. Gschneidner, J.-C. Bünzli, and V. Pecharsky (North Holland Publishing, Amsterdam, 2004), Vol. 34, Chap. 219, p. 135.
[79] R. Feyerherm, A. Amato, F. N. Gygax, A. Schenck, C. Geibel, F. Steglich, N. Sato, and T. Komatsubara, Phys. Rev. Lett. **73**, 1849 (1994).
[80] S. Sakarya, P. C. M. Gubbens, A. Yaouanc, P. Dalmas de Réotier, D. Andreica, A. Amato, U. Zimmermann, N. H. van Dijk, E. Brück, Y. Huang, and T. Gortenmulder, Phys. Rev. B **81**, 024429 (2010).
[81] A. Schenck, P. Birrer, F. N. Gygax, B. Hitti, E. Lippelt, M. Weber, P. Böni, P. Fischer, H. R. Ott, and Z. Fisk, Phys. Rev. Lett. **65**, 2454 (1990).
[82] R. Troć, M. Samsel-Czekała, E. Talik, R. Wawryk, Z. Gajek, and M. Pasturel, Phys. Rev. B **92**, 104427 (2015).
[83] A. Palacio Morales, A. Pourret, G. Knebel, G. Bastien, V. Taufour, D. Aoki, H. Yamagami, and J. Flouquet, Phys. Rev. B **93**, 155120 (2016), and references therein.
[84] M. Biasini and R. Troć, Phys. Rev. B **68**, 245118 (2003).
[85] J. Qi, T. Durakiewicz, S. A. Trugman, J. X. Zhu, P. S. Riseborough, R. Baumbach, E. D. Bauer, K. Gofryk, J.-Q. Meng, J. J. Joyce, A. J. Taylor, and R. P. Prasankumar, Phys. Rev. Lett. **111**, 057402 (2013).
[86] Y. Inada, T. Honma, N. Kawamura, M. Suzuki, H. Miyagawa, E. Yamamoto, Y. Haga, T. Okane, S. Fujimori, and Y. Ōnuki, Phys. B **359-361**, 1054 (2005).
[87] T. Okane, J. Okamoto, K. Mamiya, S. Fujimori, Y. Takeda, Y. Saitoh, Y. Muramatsu, A. Fujimori, Y. Haga, E. Yamamoto, A. Tanaka, T. Honma, Y. Inada, and Y. Ōnuki, J. Phys. Soc. Jpn. **75**, 024704 (2006).
[88] H. Sagayama, K. Kuwahara, K. Iwasa, M. Kohgi, Y. Haga, Y. Ōnuki, K. Kakurai, M. Nishi, K. Nakajima, and N. Aso, J. Phys. Soc. Jpn. **70** (Suppl. A), 28 (2001); K. Kuwahara, H. Sagayama, K. Iwasa, M. Kohgi, Y. Haga, Y. Ōnuki, K. Kakurai, M. Nishi, K. Nakajima, N. Aso, and Y. Uwatoko, Phys. B **312-313**, 106 (2002).